ACS Catalysis

Research Article

pubs.acs.org/acscatalysis

Competition between CO_2 Reduction and H_2 Evolution on Transition-Metal Electrocatalysts

Yin-Jia Zhang,[†] Vijay Sethuraman,[‡] Ronald Michalsky,[‡] and Andrew A. Peterson*[,‡]

[†]Department of Chemistry, Brown University, 324 Brook Street, Providence, Rhode Island 02912, United States

[‡]School of Engineering, Brown University, 184 Hope Street, Providence, Rhode Island 02912, United States

Supporting Information

ABSTRACT: The well-known hydrogen evolution reaction (HER) volcano plot describes the relationship between H binding energy and the corresponding hydrogen evolution catalytic activity, which depends on the species of metal. Under CO_2/CO reduction conditions or in cases where CO impurities enter electrodes, the catalyst may exist under a high coverage of coadsorbed CO. We present DFT calculations that suggest that coadsorbed CO during hydrogen evolution will weaken the binding strength between H and the catalyst surface. For metals on the right-hand side (too weak of hydrogen binding) this should lead to a suppression of the HER, as has been reported for metals such as Cu and Pt. However, for metals on the left-hand side of the volcano (too strong of hydrogen binding), this may actually enhance the kinetics of the hydrogen evolution reaction, although this effect will be countered by a decreased availability of sites for HER, which are blocked by CO. We performed experiments in Ar and CO_2 environments of two representative metals that bind CO on the far right- and left-hand side of the volcano, namely, Cu and Mo (respectively). On Cu, we find that the CO_2 environment suppresses HER, which is consistent with previous findings. However, on Mo we find that the CO_2 environment enhances HER in the kinetically active region. This helps to explain the outstanding performance of copper in CO_2 reduction and suggests that searches for high-selectivity CO_2/CO reduction catalysts may benefit from focusing on the right-hand side of the HER volcano. This also suggests principles for assessing the activity of catalysts for fuel cell and electrolysis reactions in which impurities such as CO may be present.

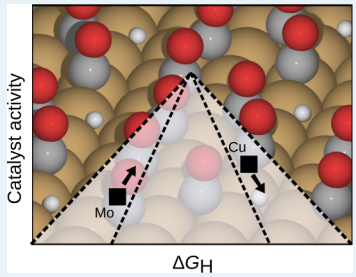

KEYWORDS: *hydrogen evolution reaction, carbon dioxide reduction, volcano plot, transition metal, DFT, promotion, poisoning*

INTRODUCTION

Electrocatalytic reactions are seen as a key technology for the energy industry, as they allow for the interconversion of chemical and electrical energy. Two key electrocatalytic reactions that can convert electrical energy into stored chemical energy are the hydrogen evolution reaction (HER) and the electrochemical reduction of CO_2. The HER continues to attract attention for many reasons. In areas where the production of hydrogen gas is desired—such as for direct fuel usage in fuel cells or rockets, or as a feedstock for Fischer–Tropsch synthesis, Haber–Bosch ammonia synthesis, or biomass hydrodeoxygenation—robust, efficient catalysts for the production of hydrogen would help to enable these processes to switch from fossil-derived H_2 to renewable H_2.[1,2] However, in some desired aqueous electrochemical processes, such as the electrocatalytic reduction of CO_2 or the electrochemical synthesis of NH_3, HER is competitive with the desired electrochemical reaction. Key products of CO_2 reduction have equilibrium potentials close to that of hydrogen evolution, for example, −0.10 V for CO and +0.08 V for C_2H_4 (both reported versus reversible hydrogen electrode, RHE, which is the equilibrium potential for HER). This suggests that adjusting the reaction thermodynamics with voltage will have limited effects on tuning the selectivity, and instead catalytic selectivity must be employed. It is challenging to control the catalytic activity for these reactions, and this requires a better understanding of the catalytic mechanism in a practical environment.

From an atomic-scale perspective, HER on a transition metal surface is considered to proceed via an adsorbed H atom intermediate by some combination of Volmer, Heyrovsky, and Tafel steps, as shown for the two series below:[3−5]

$$2H^+ + 2e^- + * \xrightarrow{\text{"Volmer"}} H^* + H^+ + e^- \xrightarrow{\text{"Heyrovsky"}} H_2 + * \quad (1)$$

$$2H^+ + 2e^- + 2* \xrightarrow{\text{"Volmer"}} 2H^* \xrightarrow{\text{"Tafel"}} H_2 + 2* \quad (2)$$

where * represents a vacant site on the surface, and H* represents a surface-bound hydrogen. In either reaction sequence, the single adsorbate of interest is a bound hydrogen atom, which suggests the binding strength of H to a catalyst surface will be a key predictor of performance.

Well before density functional theory (DFT) calculations were available to predict hydrogen bonding strength to surfaces, a volcano-shaped relation was suggested between the experimentally observed HER catalytic ability and the measured hydrogen adsorption heat;[6−8] in recent years, this was confirmed to be related to the strength of hydrogen bonding

Received: June 11, 2014
Published: September 23, 2014

   dx.doi.org/10.1021/cs5012298 | ACS Catal. 2014, 4, 3742−3748

to the catalyst surface as calculated with electronic structure methods.[9−11] In the later works, DFT was employed to calculate the chemisorption energies on a variety of metals and relate it to the HER exchange current density from experiment. The correlation shows a "volcano plot" with Pt near the peak region where the H adsorption free energy is close to zero. This relationship can be explained by the Sabatier principle, which states that the interaction between a catalyst and the reaction intermediates should be "not too strong" and "not too weak" in order to give the best performance. In the case of HER, if H adsorbs to a surface too strongly, desorption steps will be slowed; if the adsorption is too weak, the energetics of forming the intermediate are difficult, which in either case results in a high overpotential requirement. This makes the binding strength of hydrogen a simple, useful descriptor of catalytic HER activity.

In addition to the catalyst composition and structure, the binding energy of a molecule on a metal surface is affected by the local surface environment. A well-known experiment carried out by Hori and co-workers[12] showed that with copper electrodes, a delay in the hydrogen evolution onset potential is evident when the atmosphere is changed from Ar to either CO or CO_2, which can be attributed to CO "poisoning" of the catalyst surface. (We note that we use the term "poisoning" to indicate a degradation in catalyst performance, not a complete elimination of catalyst activity.) Because both CO_2 and CO lead to the delayed onset of HER, this is in agreement with many experimental and theoretical studies that suggest that CO is the primary intermediate in CO_2 electroreduction;[13−20] in other words, it is the presence of coadsorbed CO on an electrode surface during HER that delays hydrogen evolution activity. CO has been known to poison fuel cell electrodes and oxygen reduction materials by adsorbing to reactive sites.[21−26] However, in some reactions, CO can act as a promoter as well: for example, it has been suggested to facilitate the coadsorption of OH on a gold surface, leading to enhanced CO self-oxidation.[27] CO also promotes methanol oxidation on gold which has been suggested to be due to enhanced C−H bond breaking.[28] Additionally, the decomposition of ethylene on an iron catalyst has been shown to be promoted by adsorbed CO, which has been attributed to CO-induced surface reconstruction.[29]

We hypothesized that the presence of coadsorbed CO will have two predominant effects on the HER activity of a metal catalyst: (1) it will weaken the binding energy of hydrogen, and thus change the exposed surface's inherent HER activity, and (2) it will block active sites, resulting in a lower portion of the catalyst surface available for HER. The former effect could either promote or poison HER, whereas the latter should only act to poison HER. We can therefore expect a material such as Cu—which sits on the right side of the HER volcano—to exhibit decreased HER activity during the process of CO_2 electroreduction, as both effects act to decrease its activity. However, materials on the left-hand side of the HER volcano may exhibit a more nuanced response, with the two effects competing. Recently, Shi et al.[30] calculated just such a weakening in the hydrogen binding energy at high CO coverages on Pt (111) and showed that this delay was consistent with experimentally observed delays in onset potentials observed for HER on Pt electrodes under CO_2 reduction conditions. They also speculated that the peak of the volcano would "shift" toward more reactive metals under high coverage conditions. Therefore, it would be interesting to understand how the CO coverage can affect the H binding energy on representative metal surfaces and to experimentally observe the response in practice.

Herein, we report theoretical and experimental approaches to explore these phenomena. We have used DFT calculations to investigate the H binding energy on copper and molybdenum surfaces in the presence of different coverages of CO; the results reveal the expected weakening in H binding energy with realistic CO coverages. We carried out electrochemical experiments with a rotating disk electrode to test limiting materials on each side of the HER volcano—namely, copper and molybdenum—in the presence of both Ar and CO_2. By presenting the polarization curves and product analyses, we show that the HER catalytic activity can have opposite responses to coadsorbates when sampling materials from opposite sides of the volcano, as is predicted from theoretical calculations.

1. METHODS

Computational Methods. Copper and molybdenum surface models were built in the Atomic Simulation Environment (ASE) and electronic structure calculations were carried out using the planewave DFT calculator dacapo[31,32] with the exchange-correlation interactions treated by the RPBE functional[33] and the core electrons treated with ultrasoft pseudopotentials.[34] The plane wave cutoff was set at 340.15 eV and the density cutoff at 500 eV with a Fermi smearing temperature of 0.1 eV. All surfaces were constructed with 3 × 3 × 3 copper atoms with the bottom two layers fixed and the top layer relaxed. Periodic boundary conditions were applied in all directions with 20 Å of vacuum used to separate vertically stacked slabs. A *k*-point sampling of (4 × 4 × 1) was used, and a dipole correction was included in the vacuum in the direction orthogonal to the slab surface. The line search BFGS algorithm was used to optimize geometric configurations until the maximum force on any unconstrained atom was less than 0.05 eV/Å. To avoid unrealistic coverage patterns that may be seen on highly stepped surfaces such as (211), we have chosen to study the low-energy close-packed (111) surface in order to estimate the effect of adsorbed CO on the binding energy of hydrogen. The (111) surface was cut from an fcc copper bulk crystal with a lattice constant of 3.7 Å, reflecting the DFT-optimized lattice parameters used in previous theoretical studies.[13] A top view of Cu (111) is shown in Figure 1.

Equation 3 was used to calculate the binding energy of a hydrogen atom adsorbed on a copper surface at various coverages of CO:

$$E_B[\mathrm{H}] \equiv E[\mathrm{H\ on\ surface\ with}\ x\ \mathrm{CO}] - (E[\mathrm{surface\ with}\ x\ \mathrm{CO}] + E_{\mathrm{ref}}[\mathrm{H}]) \quad (3)$$

$E[\mathrm{H\ on\ surface\ with}\ x\ \mathrm{CO}]$ is the electronic energy with one H atom adsorbed at the preferred site on the copper surface surrounded by x CO molecules, in the range x = 0, 1, 2, 3, and 4. A large configurational space exists for high-coverage configurations, especially for distinguishable adsorbates. To increase the probability of finding the global minimum configuration, we took a two-pronged approach: (1) We used "brute intuition" by examining a large number of probable initial adsorption site combinations, and (2) we used the constrained minima hopping method[35,36] to independently search for low-energy configurations. Details on the range of resulting energies are provided in the Supporting Information, as are full details on the constrained minima hopping method

dx.doi.org/10.1021/cs5012298 | ACS Catal. 2014, 4, 3742−3748

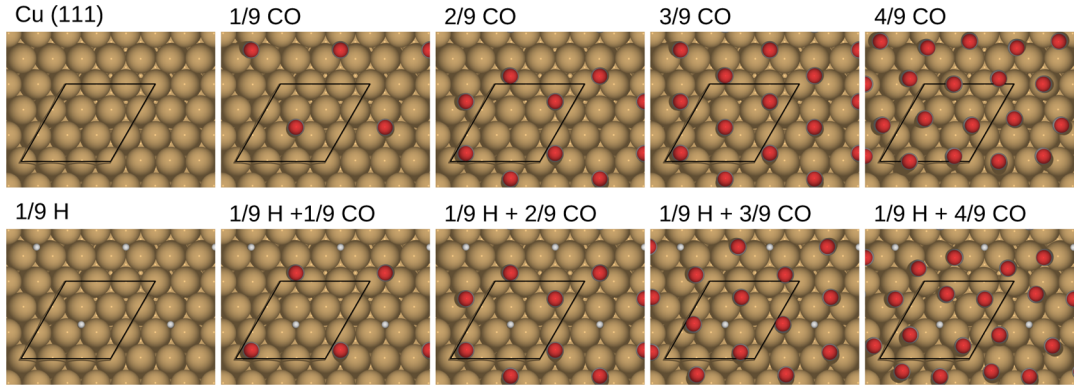

Figure 1. Cu(111) surface with H adsorbates and neighboring CO spectators at the calculated thermodynamic stable configurations. Black lines indicate the size of the unit cell. The gray atoms are carbon; red are oxygen; white are hydrogen.

employed. E[surface with x CO] is the electronic energy after the hydrogen atom is removed and the system is optimized to the nearest local minimum.

As the coverage of H was kept constant at 1/9 ML, the binding energy of H refers explicitly to the only H atom in each unit cell. For CO, we use the concept of incremental binding energy to quantify the energy changes associated with additional adsorbates. The incremental binding energy of CO without H was calculated as shown in eq 4:

$$E_B[\mathrm{CO}] \equiv E[x\ \mathrm{CO\ on\ surface}] - (E[(x-1)\ \mathrm{CO\ on\ surface}] + E_{\mathrm{ref}}[\mathrm{CO}]) \quad (4)$$

E[x CO on surface] is the electronic energy of the most thermodynamically stable configuration with x CO's on the copper surface. $E[(x-1)$ CO on surface] is the electronic energy of the most stable configuration with $(x-1)$ CO's (rather than the reoptimized configuration after removing one of the CO adsorbates). Instead of referring to a specific CO adsorbate, the incremental binding energy only considers the most thermodynamically stable situations for different coverages of CO.

Experimental Methods. *RDE Voltammetry.* Cyclic voltammetry (CV) experiments were carried out with a rotating disk electrode (RDE) (Pine Research Instrumentation) in a three-electrode cell at room temperature. The working electrode was a pure, polycrystalline bulk metal disk electrode with a rotation rate of 2000 rpm. Bulk copper (Kurt J. Lesker Company, 99.99%) and molybdenum (Kurt J. Lesker Company, 99.95%) were manufactured as a disk by the Joint Engineering/Physics Instrument Shop at Brown University to fit the rotator with the same shape and a surface area of 0.196 cm^2. The reference electrode employed was Ag/AgCl in 4 M KCl (Pine Research Instrumentation) and the counter electrode was a Pt wire. The electrolyte was a potassium phosphate buffer containing 0.1 M KH_2PO_4 (Sigma-Aldrich, ≥ 98%) and 0.1 M K_2HPO_4 (Sigma-Aldrich, ≥ 98%) prepared with ultrapure deionized water from Millipore. The electrolyte was pre-electrolyzed for more than 17 h with a 3 × 4 cm^2 graphite foil (Alfa Aesar, 99.8% metals basis) as a cathode at a current density of 0.025 mA/cm^2 in an argon atmosphere. After pre-electrolysis, experiments were carried out at a fixed potential (−0.9 V vs Ag/AgCl in 4 M KCl) on a clean graphite foil working electrode to be sure that the current did not increase with time, as an indicator of the removal of impurity metal ions. All reported voltages were adjusted to the RHE scale by adding 0.202 V to convert from Ag/AgCl (4 M KCl) to SHE and 0.059 V/pH unit to convert from the working pH to RHE. The measured pH of the buffered solution was 6.8 under Ar saturation and 6.7 under CO_2 saturation.

To keep the metal surface smooth and the surface area fixed, the working electrode was polished carefully with (in order) P600, P4000 sandpaper; 9 μm, 6 μm, 3 μm, 1 μm diamond slurry; and 0.3 μm, 0.05 μm alumina slurry; then finally washed with deionized water before each experiment. Polarization curves were obtained via a potentiostat (Autolab) in two different atmospheres, Ar (Corp Brothers, 99.999%) and CO_2 (Corp Brothers, 99.999%). To presaturate the solution, gas was bubbled for 10 min with a 0.25 L/min (20 °C, 101325 Pa) flow rate before applying potentials and kept bubbling during voltammetry. To remove any trace oxides on the working electrode, five CV cycles from −0.7 V to −1.4 V versus Ag/AgCl (4 M KCl) were scanned first at a scanning rate of 50 mV/s, after which the polarization curves were stable and repeatable. Following, another five CV cycles were scanned at a lower scan rate of 5 mV/s, and the average value of the last three cycles is reported.

Electrolysis and Product Characterization. To determine the partial current density of HER (since CO_2 is also reduced at these potentials), electrochemical reduction products near onset potentials in both the gas and liquid phase were analyzed for composition and Faradaic balance. Gas chromatography (Agilent 7890A) with both flame ionization and thermal conductivity detectors (FID and TCD) was used to detect gas-phase products and 1D ^{1}H NMR (400 MHz Avance III Ultrashield) was used to analyze liquid-phase products. As gas products generated from the tiny area of an RDE electrode at low current densities are difficult to observe quantitatively with a GC, electrolysis experiments were conducted on a 4 cm^2 metal sheet working electrode (Cu: Sigma-Aldrich, 99.98%, Mo: ESPI Metals, 99.98%) in a typical H-shaped electrolysis cell, in which the working electrode and the counter electrode were separated by a Nafion membrane (Nafion NRE-212, thickness 0.05 mm). The reference electrode in these experiments was also Ag/AgCl (4 M KCl) (Pine Research Instrumentation) and the counter electrode was a Pt wire. The electrolyte solution was the same as that in RDE experiments. The working electrode compartment was stirred by a magnetic stirrer at 1600 rpm during electrolysis. Gas products were injected into the GC via a loop injector in a six-way valve at 10, 15, and 20 min during electrolysis and the average H_2 concentration (volume percentage) is reported. Faradaic

dx.doi.org/10.1021/cs5012298 | ACS Catal. 2014, 4, 3742−3748

efficiency (yield on a per-electron basis) of H_2 was calculated via the standard definition:

$$\text{FE of } H_2(\%) \equiv \frac{\text{electrons transferred to generate } H_2}{\text{total electrons consumed}} = \frac{\text{flow rate} \times \text{time} \times \%\text{volume} \times \frac{\text{gas density}}{\text{molar mass}} \times \gamma \times F}{\text{charge}} \quad (5)$$

where the volume percentage (% volume) was determined by GC, F depicts the Faraday constant, and γ represents the number of electrons transferred per mole of gas product, which is two for H_2.

The final electrolyte after electrolysis was collected and prepared as an NMR sample. For NMR characterization, 700 μL of electrolyte and 35 μL of D_2O with 10 mM dimethyl sulfoxide (DMSO) internal standard were mixed.[37]

2. RESULTS AND DISCUSSION

To estimate the expected change in the binding strength of hydrogen on a surface crowded with carbon monoxide, we examined the thermodynamically most stable (111) facet of Cu, as shown in Figure 1. In this figure, we show the stable geometric configurations of different coverages of CO in the presence and absence of a coadsorbed H atom. A minimum surface coverage of CO under reactive conditions can be estimated by examining the top row of this figure. CO binds to the copper surface through its carbon atom and energetically favors fcc 3-fold sites. At high coverages (starting above 3/9 ML), some CO molecules are forced to occupy on-top and bridge sites as well. Quantitatively, the gray line in Figure 2 shows how the incremental CO binding energy weakens with increasing coverage; this trend follows the qualitative understanding from the discussion above. When CO coverage is less than 3/9 ML, the incremental binding energy of an added CO maintains approximately constant as 3-fold sites are still available. When CO coverage becomes greater than 3/9 ML, the binding strength of CO begins to weaken. Although a sophisticated coverage-dependent microkinetic or kinetic Monte Carlo model would be needed to make quantitative predictions of the CO coverage under reactive conditions, from the current data we can infer that the CO coverage is *at least* 3/9 ML in CO_2 reduction, as CO hydrogenation is the limiting step for CO_2 reduction,[13] and its binding energy does not weaken until after 3/9 ML coverage is reached. We note that we are inferring bounds on coverage from the DFT calculation results in a very careful way. We do not use the DFT calculations to suggest exact equilibrium coverages of CO, but use them to provide some guidance, such as "at least" 3/9 ML coverage of CO can form on copper. This prediction is quite consistent with experimental studies on CO adsorption thermodynamics: for example, a 1/3 ML coverage of CO was found in LEED experiment with a pattern of $(\sqrt{3} \times \sqrt{3})R30°$ at a low-pressure exposure of 2.7×10^{-6} Pa.[38] An analysis of CO adsorption isotherms showed that the isosteric heat of adsorption decreases abruptly when CO coverage is larger than 0.35 ML, which means that further adsorption will be weaker.[39] These results are consistent with our interpretation of the DFT data.

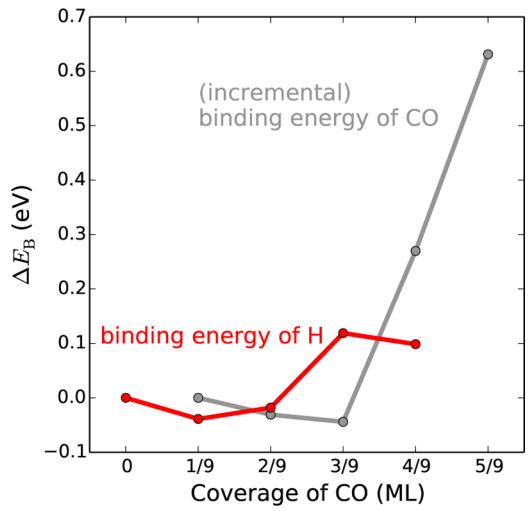

Figure 2. Relationship of incremental CO binding energy and CO coverage on Cu (gray) and the relationship of H binding energy and CO coverage Cu (red), both shown on the (111) surface. The binding energies of both CO and H are reported relative to the values on the clean copper surface: ΔE_B is defined as $\Delta E_B = E_B - E_B$[H or CO on clean surface]. The more positive ΔE_B is on the y axis, the weaker the adsorbate binds to the copper surface.

When considering interactions between coadsorbed carbon monoxide and hydrogen, it is rational to investigate configurations with a higher coverage of CO than H due to the much stronger binding of CO (relative to $CO_{(g)}$) than H (relative to 1/2 $H_{2(g)}$) on copper. To assess this, we can examine the coverage behavior of 1/9 ML of H in the presence of various coverages of CO, as shown in the second row in Figure 1. The quantitative result of this is shown as the red curve in Figure 2 in which binding energy of hydrogen is shown as a function of the coverage of coadsorbed CO molecules. The H binding strength is nearly constant at very low coverages, but when CO coverage reaches or exceeds 3/9 ML, the binding strength of H is weakened by 0.12 eV compared to that on a clean copper surface. This weakening effect can be expected to affect the HER catalytic activity of copper, and is of the same order of magnitude as is predicted by the computational hydrogen electrode model[10,40] to shift the voltage by the amount (~0.1 V) experimentally observed by Hori[12] and replicated in our measurements reported below.

Relative to an ideal HER catalyst such as platinum, numerous analyses have shown that copper binds hydrogen too weakly for optimum performance; as discussed in the introduction, it sits on the right-hand side of the well-known HER volcano,[8,10,41] and we can expect two competing effects on HER catalysis: (1) a weakening of the bonding of hydrogen to the surface, which could act to either promote or poison the HER, and (2) physical site blocking, decreasing the available surface area for the reaction. In the case of Cu, we would expect both effects to be deleterious to HER. Indeed, previous studies from the research group of Hori have shown this poisoning effect, in which the onset potential in CO_2 or CO is more negative than that in an inert argon atmosphere.[12] As transition metals share similar electronic configurations, we would assume that the weakening effect on H chemisorption strength can apply to other transition metals besides copper. In that case, CO on transition metals on the right-hand side of volcano plot will inhibit HER, like copper; while CO on transition metals on the left-hand side of the volcano—like molybdenum, which sits far to the left—should promote the kinetics of hydrogen evolution via weakening the binding between the H atom and the metal surface. But for metals on the left-hand side, the promotion

dx.doi.org/10.1021/cs5012298 | ACS Catal. 2014, 4, 3742−3748

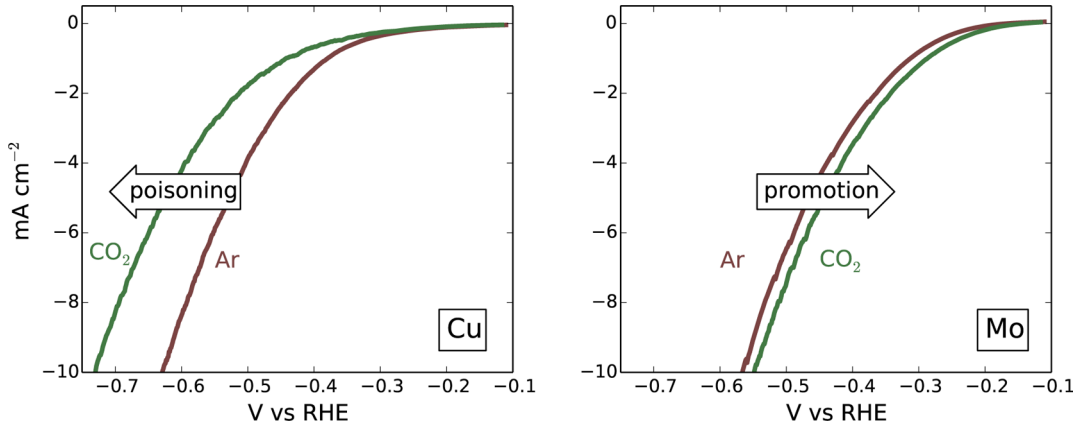

Figure 3. Polarization curves of Cu and Mo in argon versus carbon dioxide atmospheres. On Cu, the known poisoning effect of CO is observed, while on Mo the opposite is seen, presumably due to a weakening of hydrogen bonding by coadsorbed CO. Average positive-going sweeps at 5 mV/s are shown. Individual full CV plots are provided in the Supporting Information.

effect from CO will be counteracted by the site-blocking effect, and the overall effect will be a competing result.

As CO adsorbs more strongly on Mo than on Cu,[42] we expect that the equilibrium coverage of CO on Mo would not be less than that on Cu. In order to confirm this, we again used the constrained minima hopping method[35] to calculate the incremental binding energy of CO, as well as the binding energy of H in the presence of CO coadsorbates. The result suggests that CO coverage on Mo should be *at least* 5/9 ML, at which point we calculate the H binding energy to be 0.18 eV weaker than on the clean Mo surface. The weakening effect on H binding caused by CO coverage was preserved on the Mo surface. Details of the calculations on Mo can be found in the Supporting Information.

In order to test for opposite effects of CO spectator species on HER, cyclic voltammetry experiments were carried out in both Ar and CO_2 atmospheres on a material from each side of the volcano plot: copper (weak binding) and molybdenum (strong binding).[41] Copper was chosen due to its relevance in CO_2 reduction and existing literature data, whereas molybdenum was chosen because of its presence on the far-left of the volcano plot, in order to increase the likelihood of observing the binding energy (promoting) effect over the competing site-blocking (poisoning) effect. In an argon environment, we can expect only hydrogen evolution to take place in the electrochemical cell. In a CO_2 environment, the reduction of protons and CO_2 should occur simultaneously at negative voltages, leading to a surface covered in CO, as discussed earlier. We chose a potential negative enough to create a high coverage of CO on the working electrode surface; our CV potential ramp was set between −0.7 V and −1.4 V versus Ag/AgCl (4 M KCl).[14,43] Given this potential range and a pH at 6.7 (in CO_2) or 6.8 (in Ar), both copper and molybdenum are stable in their metal phase according to Pourbaix diagrams (Supporting Information). In order to compare the potentials under CO-poisoned surfaces (rather than examining the competing kinetics of CO formation on the surface), we show the positive-going sweep curves, comprising the scan from a more negative potential to a more positive potential, to decisively make the comparison between two gas environments.

Figure 3 shows polarization curves measured with a rotating disk electrode in phosphate buffer for both Cu and Mo electrodes. For copper, we can clearly see a delay in the rise of the current density in CO_2 relative to that in Ar; the presence of adsorbed CO apparently suppresses the total current. This result is consistent with Hori's previous work and our above hypothesis that a high coverage of CO on copper should inhibit the HER activity. For molybdenum, the onset potential of HER is around −0.3 V versus RHE and the current density in CO_2 is clearly larger than that in Ar at potentials around the onset potential. When the voltage is more negative, both the current in Ar and in CO_2 increase rapidly, but the current in CO_2 stays larger. The promotion effect occurs in the CO_2 environment, implying a coverage of CO enhances the HER. As the promotion effect is accompanied by the site-blocking effect by CO, the current density gap on Mo is much smaller than that on Cu.

Although Figure 3 shows changes to the total current, it is conceivable that much of the current could be due to the reduction of CO_2 itself, not the production of H_2. To verify the composition of products in the range around the onset potentials, gas products were analyzed by gas chromatography (GC) to determine the Faradaic efficiency for hydrogen. Because both the current density at onset potentials and the RDE working electrode surface area (0.196 cm^2) are small, it is difficult to reproducibly close a Faradaic balance at these conditions. To provide a more quantitative measure of the product yields, electrolysis was conducted in a two-chamber electrochemical cell with a metal sheet as a working electrode with a much larger surface area of 4 cm^2. Potentiostatic experiments were conducted with copper foil electrodes at −0.4 V versus RHE in both Ar and CO_2, whereas potentiostatic Mo experiments were conducted at −0.3 V versus RHE, both chosen to approximate their onset potentials. Before each electrolysis measurement, five cycles of polarization from −0.7 V to −1.4 V versus Ag/AgCl (4 M KCl) were first scanned at a scanning rate of 50 mV/s to provide a coverage of CO during electrolysis in experiments containing CO_2. The H_2 Faradaic efficiency was calculated using the H_2 concentration determined by GC in each test.

All the results are summarized in Table 1; for both Cu and Mo, the FE of hydrogen is nearly the same in Ar and in CO_2 (i.e., close to 100%). Within the detection limit of the GC, the previously reported gas products for CO_2 reduction on Cu surfaces at more negative potentials were not observed at −0.3 V versus RHE, such as CH_4, C_2H_4, and CO.[14,37] (Note that this is consistent with reports showing at low current densities, Cu produces mainly H_2, not CO_2 reduction

dx.doi.org/10.1021/cs5012298 | *ACS Catal.* 2014, 4, 3742−3748

Table 1. GC Analysis of Gas Products for Cu and Mo

metal	potential (V vs RHE)	gas environment	H_2 FE (%)
Cu	−0.4	Ar	99.9
	−0.4	CO_2	97.7
Mo	−0.3	Ar	100.6
	−0.3	CO_2	100.0

products.) For Mo, only H_2 was found in both Ar and CO_2 atmospheres during the reduction reaction, which is consistent with previous researchers' reports.[44,45] The liquid-phase electrolyte collected after 1 h of electrolysis was analyzed by 1D ^{1}H NMR. No carbon-containing chemical peaks were found for either Cu or Mo. Therefore, it can be concluded that at the onset potentials for Cu and Mo, predominantly hydrogen is generated and contributes the vast majority of the current even in CO_2 atmosphere, suggesting the validity of interpreting the shifts in polarization curves as shifts in the effectiveness of the catalyst for hydrogen evolution.

In the discussion above, we have presented data that confirms findings from the literature showing the HER current on Cu is markedly reduced in a CO_2 atmosphere as compared to Ar; this correlates with electronic structure calculations that confirm the magnitude and direction of this shift. Conversely, we show that Mo—which sits on the left-hand, or strong binding, side of the HER volcano—shows just the opposite response, which can be explained by the weakening of the surface−hydrogen bond, pushing the catalyst into a more favorable position with respect to the peak of the HER volcano. Even at more negative voltages than the onset potential, the above trend remains intact in spite of other factors such as mass transport limitations, the beginning of CO_2 reduction, and the site-blocking effect of CO. Thus, the experimental results support the theoretical suggestion that a high coverage of CO will weaken the binding of H on transition metal surfaces and this effect (in combination with other effects) can either decrease or increase the hydrogen evolution current density, depending on the metal's position in the volcano plot.

3. CONCLUSIONS

The presence of coadsorbates can have nontrivial effects on the efficacy of a catalyst for the hydrogen evolution reaction, as calculated in binding energy changes and experimentally suggested by changes in the performance of Cu and Mo in electrochemical CO_2 reduction. Our DFT calculations show that the binding energy of H weakens with increasing coverages of CO on both the Cu fcc(111) and Mo bcc(110) surface. Specifically, it was calculated that the binding strength of a hydrogen atom will be weakened by about 0.12 eV when the CO coverage is 3/9 ML on Cu, which is a minimal CO coverage we might expect for CO_2 reduction at room temperature and atmospheric pressure. On Mo surfaces, we expect a higher coverage of CO and an even greater weakening of the hydrogen binding energy. This weakening effect on H atom binding strength is expected to inhibit HER activity on metals on the right-hand side of the volcano plot (e.g., copper) and promote HER on metals on the left-hand side (e.g., molybdenum). This is combined with other effects, such as site blocking, that will change the kinetics of hydrogen evolution; experimentally, it is difficult to distinguish between the weakening effect on hydrogen binding strength discussed above and other effects. The site-blocking effect can be expected to enhance the poisoning effect on copper and undermine the promotion effect on molybdenum. Despite this, our CV experiments and product analyses have clearly shown that CO_2 reduction conditions suppress HER on copper and improve HER on molybdenum.

The poisoning effect on HER from coadsorbed CO can give us some insights into the unique performance of copper in CO_2 reduction. In aqueous electrolytes, the reduction of CO_2 and the reduction of protons (to H_2) are competing reactions. A high coverage of CO intermediates not only increases the rate of CO_2 reduction but also reduces the catalyst's ability in hydrogen evolution. This is a critical reason why copper is so selective in CO_2 reduction at negative potentials: it is reactive enough to bind CO but still noble enough to sit on the right-hand side of the HER volcano. This suggests a design principle: that future searches for optimum CO_2 reduction catalysts may benefit from not only focusing on catalysts that are poor for HER, but that preferentially sit on the right-hand side of the HER volcano plot.

This also suggests the intriguing possibility that in the search for nonprecious hydrogen evolution and hydrogen oxidation catalysts, one may want to deliberately poison the catalyst rather than scrupulously avoid it.

■ ASSOCIATED CONTENT

Supporting Information

Details of all configurations tested in DFT calculations, the constrained minima hopping methodology, calculation results on Mo surface, individual CV plots for Cu and Mo RDE, CV plots of metal sheets and Pourbaix diagrams are included. This material is available free of charge via the Internet at http://pubs.acs.org.

■ AUTHOR INFORMATION

Corresponding Author

*E-mail: andrew_peterson@brown.edu. Tel.: +1 401-863-2153.

Notes

The authors declare no competing financial interest.

■ ACKNOWLEDGMENTS

We gratefully acknowledge financial support from the Young Investigator Award from the Office of Naval Research under award N00014-12-1-0851. Calculations were undertaken at the Center for Computation and Visualization (CCV), Brown University.

■ REFERENCES

(1) Nørskov, J. K.; Bligaard, T.; Rossmeisl, J.; Christensen, C. H. *Nat. Chem.* **2009**, *1*, 37−46.
(2) Li, Y.; Wang, H.; Xie, L.; Liang, Y.; Hong, G.; Dai, H. *J. Am. Chem. Soc.* **2011**, *133*, 7296−7299.
(3) Saraby-Reintjes, A. *Electrochim. Acta* **1986**, *31*, 251−254.
(4) Gennero de Chialvo, M.; Chialvo, A. *Electrochim. Acta* **1998**, *44*, 841−851.
(5) Koper, M. T. *J. Electroanal. Chem.* **2011**, *660*, 254−260.
(6) Conway, B. E.; Bockris, J. O. *J. Chem. Phys.* **1957**, *26*, 532−541.
(7) Parsons, R. *Trans. Faraday Soc.* **1958**, *54*, 1053−1063.
(8) Trasatti, S. *J. Electroanal. Chem. Interfacial Electrochem.* **1972**, *39*, 163−184.
(9) Orita, H.; Uchida, K.; Itoh, N. *Appl. Catal., A* **2004**, *258*, 115−120.
(10) Nørskov, J. K.; Bligaard, T.; Logadottir, A.; Kitchin, J.; Chen, J.; Pandelov, S.; Stimming, U. *J. Electrochem. Soc.* **2005**, *152*, J23−J26.

(11) Skúlason, E.; Tripkovic, V.; Björketun, M. E.; Gudmundsdóttir, S.; Karlberg, G.; Rossmeisl, J.; Bligaard, T.; Jónsson, H.; Nørskov, J. K. *J. Phys. Chem. C* **2010**, *114*, 18182−18197.
(12) Hori, Y.; Murata, A.; Takahashi, R. *J. Chem. Soc., Faraday Trans. 1* **1989**, *85*, 2309−2326.
(13) Peterson, A. A.; Abild-Pedersen, F.; Studt, F.; Rossmeisl, J.; Nørskov, J. K. *Energy Environ. Sci.* **2010**, *3*, 1311−1315.
(14) Hori, Y. In *Modern Aspects of Electrochemistry*; Vayenas, C. G., White, R. E., Gamboa-Aldeco, M. E., Eds.; Springer: New York, 2008; Vol. *42*, pp 89−189.
(15) Hori, Y.; Murata, A.; Takahashi, R.; Suzuki, S. *J. Am. Chem. Soc.* **1987**, *109*, 5022−5023.
(16) Kim, J. J.; Summers, D. P.; Frese, K. W. J. R. *J. Electroanal. Chem.* **1988**, *245*, 223−244.
(17) DeWulf, D. W.; Jin, T.; Bard, A. J. *J. Electrochem. Soc.* **1989**, *136*, 1686−1691.
(18) Peterson, A. A.; Nørskov, J. K. *J. Phys. Chem. Lett.* **2012**, *3*, 251−258.
(19) Schouten, K. J. P.; Kwon, Y.; van der Ham, C. J. M.; Qin, Z.; Koper, M. T. M. *Chem. Sci.* **2011**, *2*, 1902−1909.
(20) Nie, X.; Esopi, M. R.; Janik, M. J.; Asthagiri, A. *Angew. Chem., Int. Ed.* **2013**, *52*, 2459−2462.
(21) Winter, M.; Brodd, R. J. *Chem. Rev.* **2004**, *104*, 4245−4270.
(22) Camara, G.; Ticianelli, E.; Mukerjee, S.; Lee, S.; McBreen, J. *J. Electrochem. Soc.* **2002**, *149*, A748−A753.
(23) Baschuk, J.; Li, X. *Int. J. Energy Res.* **2001**, *25*, 695−713.
(24) Götz, M.; Wendt, H. *Electrochim. Acta* **1998**, *43*, 3637−3644.
(25) Yang, L.; Jiang, S.; Zhao, Y.; Zhu, L.; Chen, S.; Wang, X.; Wu, Q.; Ma, J.; Ma, Y.; Hu, Z. *Angew. Chem.* **2011**, *123*, 7270−7273.
(26) Oetjen, H.-F.; Schmidt, V.; Stimming, U.; Trila, F. *J. Electrochem. Soc.* **1996**, *143*, 3838−3842.
(27) Rodríguez, P.; Koverga, A. A.; Koper, M. *Angew. Chem., Int. Ed.* **2010**, *49*, 1241−1243.
(28) Rodríguez, P.; Kwon, Y.; Koper, M. T. *Nat. Chem.* **2012**, *4*, 177−182.
(29) Rodriguez, N.; Kim, M.; Baker, R. *J. Catal.* **1993**, *144*, 93−108.
(30) Shi, C.; Hansen, H. A.; Lausche, A. C.; Nørskov, J. K. *Phys. Chem. Chem. Phys.* **2014**, *16*, 4720−4727.
(31) Bahn, S.; Jacobsen, K. *Comput. Sci. Eng.* **2002**, *4*, 56−66.
(32) The DACAPO plane wave/pseudopotential DFT code is available as open source software at http://www.fysik.dtu.dk/CAMPOS/.
(33) Hammer, B.; Hansen, L. B.; Nørskov, J. K. *Phys. Rev. B* **1999**, *59*, 7413−7421.
(34) Vanderbilt, D. *Phys. Rev. B* **1990**, *41*, 7892−7895.
(35) Peterson, A. A. *Top. Catal.* **2014**, *57*, 40−53.
(36) Goedecker, S. *J. Chem. Phys.* **2004**, *120*, 9911−9917.
(37) Kuhl, K. P.; Cave, E. R.; Abram, D. N.; Jaramillo, T. F. *Energy Environ. Sci.* **2012**, *5*, 7050−7059.
(38) Pritchard, J. *J. Vac. Sci. Technol.* **1972**, *9*, 895−900.
(39) Truong, C. M.; Rodriguez, J.; Goodman, D. *Surf. Sci.* **1992**, *271*, L385−L391.
(40) Nørskov, J. K.; Rossmeisl, J.; Logadottir, A.; Lindqvist, L.; Kitchin, J. R.; Bligaard, T.; Jonsson, H. *J. Phys. Chem. B* **2004**, *108*, 17886−17892.
(41) Greeley, J.; Jaramillo, T. F.; Bonde, J.; Chorkendorff, I.; Nørskov, J. K. *Nat. Mater.* **2006**, *5*, 909−913.
(42) Clarke, L. *Surf. Sci.* **1981**, *102*, 331−347.
(43) Summers, D. P.; Leach, S.; F, K. W., Jr. *J. Electroanal. Chem. Interfacial Electrochem.* **1986**, *205*, 219−232.
(44) Noda, H.; Ikeda, S.; Oda, Y.; Imai, K.; Maeda, M.; Ito, K. *Bull. Chem. Soc. Jpn.* **1990**, *63*, 2459−2462.
(45) Hara, K.; Kudo, A.; Sakata, T. *J. Electroanal. Chem.* **1995**, *391*, 141−147.